powders

MDPI

Article

Effects of Auto-Stirring on Powder Dispensing Rate Consistency in Hopper-Based Binder Jetting 3D Printing with Cohesive Powder

Jackson Sanders [1,*], Siddhartha Kazi [1], Zhijian Pei [1], Yi-Tang Kao [2] and Kenneth Dubovick [2]

[1] Department of Industrial & Systems Engineering, Texas A&M University, College Station, TX 77843, USA; siddharthakazi@gmail.com (S.K.); zjpei@tamu.edu (Z.P.)
[2] Saint-Gobain Research North America, Northborough, MA 01532, USA; ken.dubovick@saint-gobain.com (K.D.)
* Correspondence: jacksonjsanders@tamu.edu

Abstract

In hopper-based binder jetting 3D printing, a consistent powder dispensing rate from the hopper to the powder bed is essential for reliable printing. This study investigates the effects of adding a custom-built auto-stirrer to the hopper system on the consistency of powder dispensing rate for the ExOne Innovent+ binder jetting 3D printer (Desktop Metal, Burlington, MA, USA). The auto-stirrer incorporates rotating augers that actively agitate the powder in the hopper. Working together with the ultrasonic vibrator, the auto-stirrer facilitates consistent dispensing of powder through the hopper outlet. Experiments with algae powder demonstrated that adding the auto stirrer reduced fluctuations in dispensing rate by over 30% compared with the standard hopper. Statistical analysis confirmed that these improvements were significant (at a significance level of 0.05). These results indicate that integrating active mechanical agitation into hopper-based powder dispensing systems could help to achieve more consistent powder dispensing rates in hopper-based binder jetting 3D printing that uses cohesive powder feedstocks.

Keywords: additive manufacturing; binder jetting 3D printing; hopper; stirring; dispensing rate; cohesive powder

1. Introduction

1.1. Powder Dispensing in Binder Jetting 3D Printing

Powder bed fusion additive manufacturing consists of several major process families, including laser powder bed fusion (LPBF), electron beam powder bed fusion (EB-PBF), and binder jetting 3D printing [1,2]. Each process fabricates parts layer by layer from a powder bed but differs in how layers are consolidated. In LPBF and EB-PBF, a laser or electron beam selectively melts and fuses powder particles, which constrains compatible feedstocks to principally metal powders with high flowability and particle morphologies suitable for wiper or roller spreading [3,4]. Binder jetting 3D printing, by contrast, bonds powder particles using a liquid binder rather than thermal fusion, enabling a broader range of feedstock materials. These materials include metals, ceramics, and highly cohesive or irregularly shaped powders that may be inaccessible to LPBF and EB-PBF.

Similar to the other powder bed fusion techniques mentioned previously, binder jetting 3D printing can be used to produce geometrically complex parts with reduced material waste and short lead times [5]. Several applications have been demonstrated

Academic Editors: Paul F. Luckham, Vivek Garg, Tong Deng and Michael Bradley

Received: 16 March 2026
Revised: 14 May 2026
Accepted: 1 June 2026
Published: 8 June 2026

across aerospace, automotive, biomedical, and energy sectors [6,7]. Layer by layer, powder is added onto a build platform to prepare a layer of powder, then powder particles in selected regions of the powder bed are subsequently bonded to create three-dimensional parts [8].

There are mainly two types of powder dispensing methods used in binder jetting 3D printing, piston-based method and hopper-based method. In the piston-based method, a spreader (roller or blade) spreads powder deposited from a piston-lifted powder supply platform onto the build platform [9,10]. This method can struggle with highly cohesive or irregularly shaped powders that resist uniform spreading from the supply platform to the build platform under the applied mechanical force of the spreader [11]. In the hopper-based method, powder is dispensed directly onto the build platform and smoothed by a roller.

To form a powder bed in a hopper-based binder jetting 3D printer, the hopper, filled with powder, traverses the build platform as a vibratory mechanism dispenses powder through a screen attached to its bottom opening [12]. Although the hopper-based method opens the door to highly cohesive powder materials potentially inaccessible to the piston-based method, issues with powder dispensing rate consistency arise. Inconsistent powder dispensing rates can cause variations in the density and surface uniformity of the powder bed across the build platform, especially when the hopper does not dispense enough powder to establish the full layer thickness across the powder bed. These variations can ultimately impact the final part's density, dimensional accuracy, and mechanical properties [13–15]. Various approaches have been reported to address the challenge of dispensing rate consistency for highly cohesive powders in hopper-based dispensing systems, but no single approach has demonstrated consistent effectiveness for binder jetting 3D printing.

1.2. Reported Approaches for Achieving Consistent Powder Dispensing Rate with Hopper-Based Dispensing Systems and Issues That Arise with Cohesive Powders

Four approaches have been reported to address powder dispensing rate consistency in hopper-based dispensing systems: vibrational assistance, particle surface modification, environmental control, and mechanical agitation. While generally effective in promoting consistent dispensing rates with nominally flowable powders, each approach presents notable limitations when applied to highly cohesive powders.

Vibrational assistance is a widely used approach to improve powder dispensing consistency in hopper-based systems where vibrations disrupt particle agglomerates and reduce cohesive forces between powder particles [16,17], thereby promoting a consistent powder dispensing rate [18]. However, vibrational assistance has limitations when applied to highly cohesive powders. Primarily, ultrasonic energy may be insufficient to overcome strong interparticle bonds in cohesive powders. As a result, flow interruptions such as bridging (where powder particles form stable arches that block the hopper outlet) and clogging (where powder accumulates and solidifies within the hopper, restricting powder flow) can still occur, leading to inconsistent dispensing rates [19].

Particle surface modification involves adding flow aids, such as fumed silica or other nano-additives, that coat the surfaces of feedstock powder particles [20]. These nano-scale coatings act as spacers between host powder particles, reducing interparticle cohesion and increasing flow properties [21–23]. However, the addition of flow aids may compromise material purity by introducing foreign substances into the feedstock, making it unsuitable for applications where material composition must remain unaltered [19]. In binder jetting 3D printing, maintaining powder chemical purity is generally critical to ensure the final printed parts have proper compositions, regardless of powder feedstock cohesivity.

Environmental control focuses on managing the temperature and humidity surrounding the powder during pre-printing preparation and/or the printing process. Drying of feedstock powder before printing at temperatures ranging from 80 to 200 °C removes

moisture from the powder and reduces cohesive forces, improving powder flow characteristics [24]. However, excessive drying can lead to flow irregularities due to electrostatic charging [25]. Additionally, while drying can improve dispensing rate consistency, the maximum improvement achievable is limited by the powder feedstock's inherent cohesivity in its dried state.

Mechanical agitation through impellers or augers disrupts stagnant zones (regions in a hopper where powder remains relatively stationary) and promotes more consistent dispensing rates [26,27]. Although this approach does prevent stagnation in the bulk of a hopper volume, cohesive powder feedstocks can still compact or bridge across the hopper's dispensing outlet, contributing to dispensing rate variation or complete flow stoppage [28]. Despite demonstrated effectiveness in other powder handling applications, mechanical agitation remains underexplored as a strategy for enhancing dispensing rate consistency in binder jetting 3D printing [29–31].

Furthermore, while vibrational assistance and mechanical agitation have been studied as independent approaches for powder dispensing rate consistency enhancement, there is limited reported research on the combination of vibrational assistance with mechanical agitation in the context of hopper-based powder dispensing [17,32]. The potential effects of combining these approaches have not been thoroughly investigated, particularly for highly cohesive powders.

1.3. Gaps in Hopper-Based Powder Dispensing Rate Research

Several significant gaps remain in the literature regarding hopper-based powder dispensing systems. Most reported studies focus on large-scale hoppers, often with capacities exceeding 250 L and outlet diameters above 20–30 cm [18,33,34]. These large-scale hoppers are used for agricultural or mining feedstocks [35–37]. Hoppers used in 3D printing typically operate with volumes below 5 L and outlet diameters of 100 µm to 5 mm [35,38,39]. Binder jetting 3D printers equipped with hoppers often dispense powder at rates down to milligram-per-second range, achieving layer thicknesses as small as 20–100 µm [17,32,40]. The requirements of the binder jetting 3D printing process, including layer thickness control and consistent material dispensing, necessitate specialized mechanisms for consistent powder dispensing. These kinds of specialized powder dispensing mechanisms have rarely been reported in the literature [17,41].

1.4. Objectives of This Study

To the authors' best knowledge, no reported study on binder jetting 3D printing has systematically evaluated dispensing rate consistency for a hopper-based powder dispensing system with integrated ultrasonic vibration and mechanical agitation. To address this gap, this study investigates the effects of a hopper-based powder dispensing system equipped with integrated ultrasonic vibration and mechanical agitation (auto-stirring) on dispensing rate consistency in binder jetting 3D printing.

The remainder of this paper is organized as follows. Section 2 details the materials and methods, including the design and operation of the auto-stir hopper system, characteristics of the cohesive algae powder feedstock, and the procedures used for evaluating dispensing rate consistency. Section 3 presents the results and discussion, focusing on the impact of auto-stirring on dispensing rate consistency. Section 4 provides the conclusions and suggests directions for future research.

2. Materials and Methods

2.1. ExOne Innovent+ Binder Jetting 3D Printer and Its Ultrasonic Hopper Dispensing System

The binder jetting 3D printing process for the ExOne Innovent+ (Desktop Metal, Burlington, MA, USA) consists of three primary steps, shown in Figure 1, repeated cyclically to create three-dimensional objects layer by layer from a digital model.

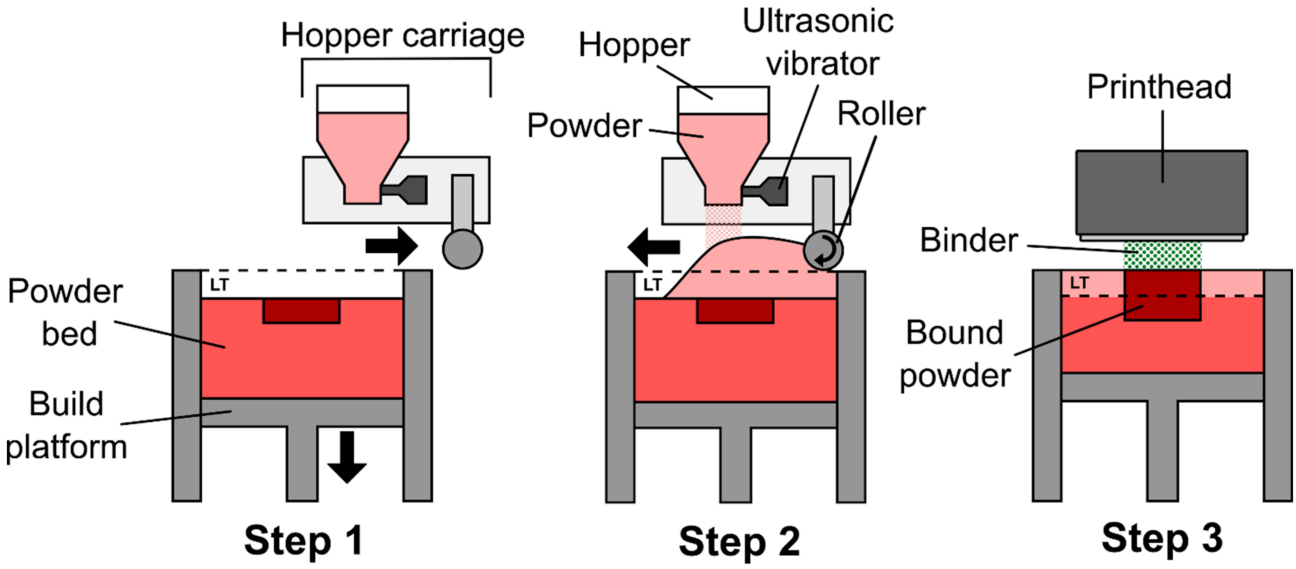

Figure 1. Illustration of the ultrasonic hopper-based binder jetting 3D printing process in three steps (LT: layer thickness).

- Step 1: The build platform lowers by the desired layer thickness (LT), creating space for a new powder layer. The hopper carriage traverses from left to right across the powder bed.
- Step 2: The hopper carriage moves from right to left. An ultrasonic vibrator attached to the hopper is activated to facilitate feedstock powder flow from the hopper onto the powder bed. The hopper dispenses more powder than needed for a single layer, while a roller spreads the powder bed, resulting in a new powder layer with the thickness of LT.
- Step 3: A printhead, independent from the hopper carriage, deposits liquid binder onto selected regions of the powder bed based on the digital model geometry. The binder bonds the powder particles within those regions and penetrates below, adhering the new layer of powder to the previously bound layers.

Steps 1–3 are repeated until the object is fully built, resulting in a finished printed part that remains surrounded by loose, unbound powder in the powder bed. Typical binder jetting 3D printing workflows involve further post-processing (such as curing, debinding, and sintering) to strengthen the printed part [2]. These steps are outside the scope of this study and are not discussed here.

The ExOne Innovent+ binder jetting 3D printer has an ultrasonic hopper dispensing system to deliver powder to the build platform. Figure 2 shows multiple views of the hopper components and assembly. The hopper is affixed to the top of the ultrasonic generator with screws, and the screen is affixed to the bottom of the ultrasonic generator with screws. A power supply is connected to the ultrasonic generator. Upon activation of the ultrasonic generator, ultrasonic vibration enables feedstock powder to be dispensed through the screen.

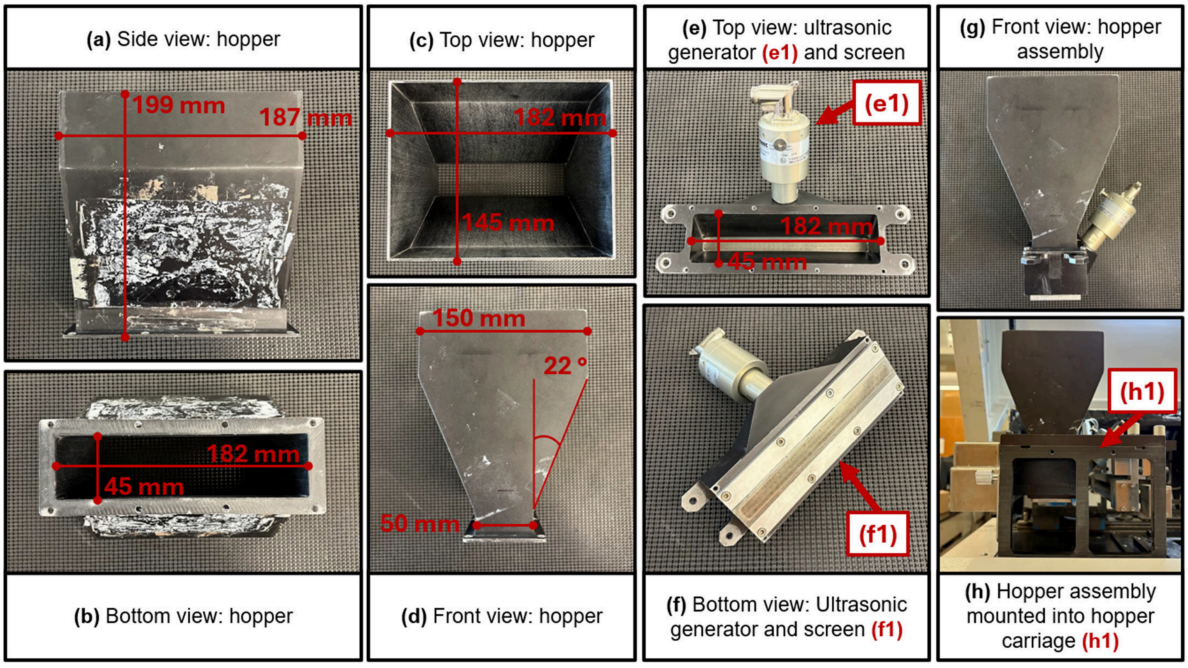

Figure 2. Powder dispensing components of the ExOne Innovent+ binder jetting 3D printer.

2.2. Auto-Stirring Device for Hopper-Based Powder Dispensing Systems

A custom hopper incorporating automatic stirring (auto-stir) capability was designed and fabricated for this study. Figure 3 presents several views of the computer-aided design (CAD) assembly excluding electronic components, while Figure 4 shows the auto-stir hopper installed in the Innovent+ binder jetting 3D printer.

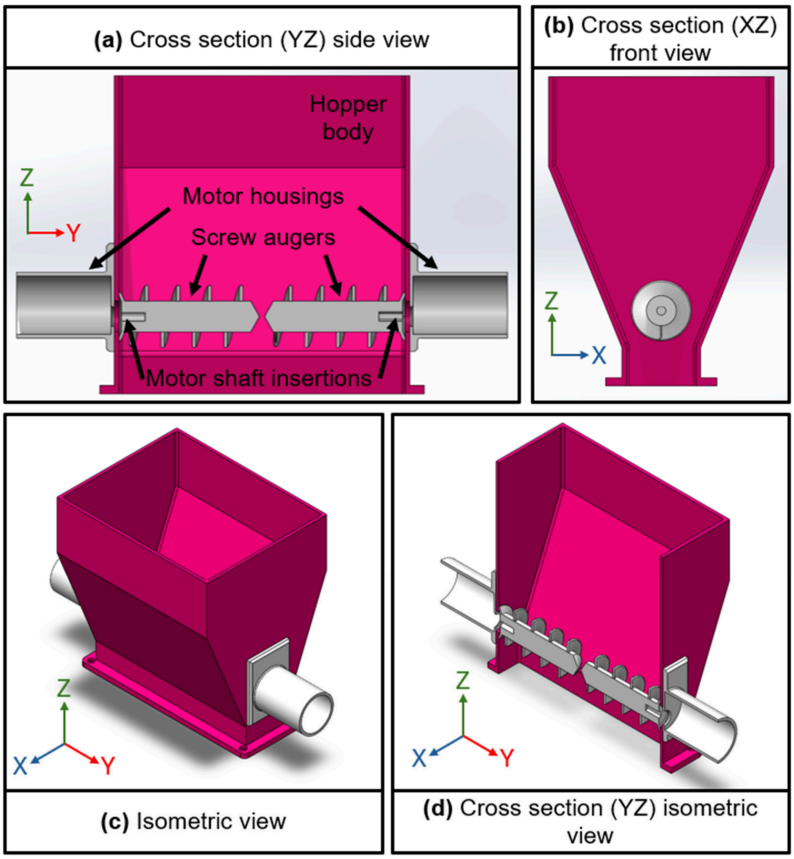

Figure 3. CAD assembly of the auto-stir hopper.

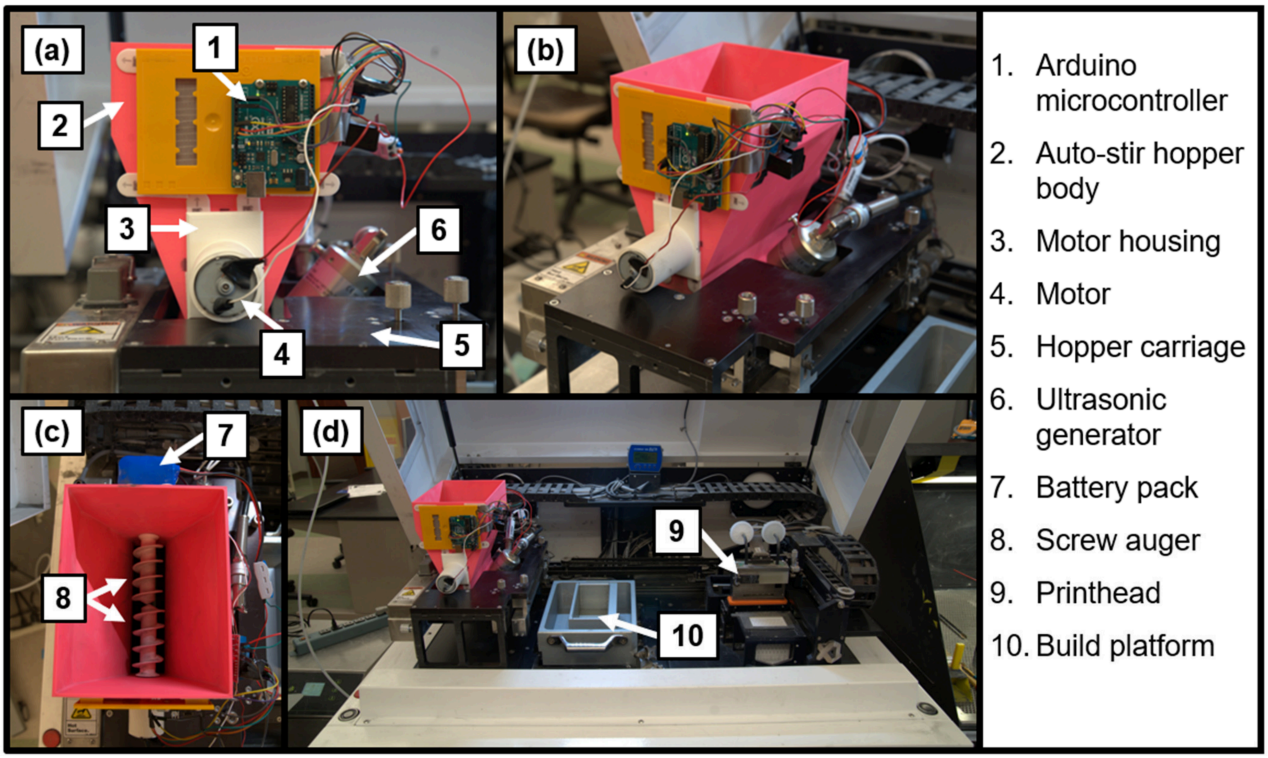

Figure 4. Views of the auto-stir hopper in the ExOne Innovent+ binder jetting 3D printer: (**a**) front view, (**b**) isometric view, (**c**) top view, and (**d**) the full printer chamber.

2.2.1. Design and Fabrication of Auto-Stir Hopper Body

A three-dimensional model replicating the dimensional specifications of the ExOne OEM hopper was created using SolidWorks 2024 student edition (Dassault Systèmes, Vélizy-Villacoublay, France). Two circular apertures (diameter = 20 mm) were designed perpendicular to the hopper's front and back faces along the Y-axis, positioned 40 mm from the base. The hopper body was manufactured via fused deposition modeling (FDM) using a CreatWare F430 3D printer (Henan Creatbot Technology Limited, Zhengzhou, HA, China) with eSUN PLA+ filament (1.75 mm diameter, pink; Shenzhen eSUN Industrial Co., Ltd., Shenzhen, GD, China).

2.2.2. Design and Fabrication of Motor Housings and Screw Auger

Press-fit motor housings were designed to align concentrically with the apertures described above. Each housing consisted of a cylindrical body (diameter = 37.6 mm, length = 60 mm) integrated with a flat mounting plate (70 mm × 50 mm, oriented vertically). Helical screw augers were designed so that the motor shafts could be inserted into the body of the screw augers with a press-fit. Each auger, standing upright, measured 89 mm in height with a cylindrical shaft diameter of 20 mm, flaring to 31 mm at the base. The helical flight was generated by sweeping a rectangular profile (10 mm × 2 mm with 0.75 mm edge fillets) along a clockwise helical path with a pitch of 20 mm, completing 3.75 revolutions. Both motor housings and augers were manufactured using a Creality Ender-6 FDM printer (Shenzhen Creality 3D Technology Co., Ltd., Shenzhen, GD, China) with PLA filament.

2.2.3. Integration of Hopper Assembly and Control System

Two motor housings were affixed to the hopper's external vertical surfaces using 3M Command Poster Strips (3M Company, St. Paul, MN, USA). Two DC torque motors (12 V, 20 RPM; Greartisan, Shenzhen, GD, China) were press-fitted into the housings, and the screw augers were subsequently attached to the motor shafts. The motor control

system consisted of an Arduino Uno R3 microcontroller (Arduino S.r.l., Monza, Italy), an L298N dual H-bridge motor driver module (WWZMDiB, Shenzhen, GD, China), and a 12 V 2400 mAh rechargeable lithium-ion battery pack (Shenzhen KangBeiTe Electronics Co., Ltd., Shenzhen, GD, China). These components were mounted to the hopper's exterior surface with Command Poster Strips. Electrical connections were established between the Arduino digital output pins and the motor driver input terminals, with subsequent connections from the motor driver output channels to the DC motors. The battery pack provided electric power to both the motor driver and Arduino board.

The Arduino microcontroller was programmed to initiate continuous counter-rotation of the screw augers upon power activation. Counter-rotation in this instance is defined in such a way that, when viewed from the front of the hopper, the front auger (closer to the observer) rotated clockwise while the rear auger rotated counterclockwise. This counter-rotating configuration generated opposing flow fields that converged toward the hopper's center, producing shear-induced mixing of the powder in the auto-stir hopper. The fully assembled auto-stir hopper installed into the Innovent+ binder jetting 3D printer is shown in Figure 4.

2.3. Feedstock Powder

The feedstock powder used was spirulina blue-green algae, sourced commercially (Carlyle Nutritionals, Melville, NY, USA). This algae powder served as a simulant of waste algae powder from the algal biofuel production process [42]. The received powder was sieved using a 250 μm sieve (ASTM No. 60) to break up agglomerates. No additives were added to the algae powder. The feedstock powder used in this study was identical to that characterized in the authors' previous work on binder jetting 3D printing with algae powder [43]. Table 1 outlines the flowability classification for powders by repose angle and Hausner ratio while Table 2 provides the physical properties and flowability metrics of the algae powder used in this study. Repose angle describes the angle formed by a freely poured heap of powder on a horizontal surface, while the Hausner ratio is the ratio of tapped to bulk density; both are commonly used indicators of powder flowability. Table 3 provides flowability metrics for commonly used metal and ceramic powders used for powder bed 3D printing.

Table 1. Classification of flowability by repose angle [44] and Hausner ratio [45].

Repose Angle	Hausner Ratio	Flowability Classification
$20° < \alpha < 30°$	1.00–1.11	Very free flowing
$30° < \alpha < 38°$	1.12–1.18	Free flowing
$38° < \alpha < 45°$	1.19–1.25	Fair flow
$45° < \alpha < 55°$	1.26–1.34	Cohesive
$55° < \alpha < 70°$	1.35–1.45	Very cohesive

Table 2. Physical properties and flowability of algae powder used in the study [43].

Property	Value
Particle size distribution (μm)	D_{10} = 65, D_{50} = 100, D_{90} = 190
Apparent density (g/cm^3)	0.45
Repose angle (°)	56
Flowability classification	Very cohesive

Table 3. Summary of properties for commonly used metal and ceramic powders for powder 3D printing.

Material	Property	Value	Reference
316 L Stainless Steel	Particle size distribution (μm)	D_{10} = 26.7 D_{50} = 42.6 D_{90} = 64.0	[44]
	Repose angle (Mean ± Std) (°)	34.2 ± 2	
	Flowability classification	Free flowing	
Aluminum	Particle size distribution (μm)	D_{10} = 29.4 D_{50} = 79.1 D_{90} = 187.3	[44]
	Repose angle (Mean ± Std) (°)	36.8 ± 1.5	
	Flowability classification	Free flowing	
Titanium	Particle size distribution (μm)	D_{10} = 80.7 D_{50} = 295.1 D_{90} = 452.1	[44]
	Repose angle (Mean ± Std) (°)	44.9 ± 1.6	
	Flowability classification	Fair flow	
Alumina (spherical)	Particle size distribution (μm)	D_{10} = 10.1 D_{50} = 21.6 D_{90} = 39.0	[46]
	Repose angle (Mean ± Std) (°)	50.3 ± 0.6	
	Flowability classification	Cohesive	
Alumina (irregular)	Particle size distribution (μm)	D_{10} = 13.4 D_{50} = 23.8 D_{90} = 41.9	[46]
	Repose angle (Mean ± Std) (°)	43.6 ± 1.8	
	Flowability classification	Fair flow	
Silicon Carbide	Particle size distribution (μm)	D_{10} = 42.2 D_{50} = 63.7 D_{90} = 93.2	[47]
	Repose angle (Mean ± Std) (°)	Not available	
	Hausner ratio	1.134	
	Flowability classification	Free flowing	

Field-emission scanning electron microscopy (SEM) revealed the powder particles to be roughly spherical to ellipsoid-shaped, with relatively uniform geometry. SEM images of the algae powder used in this study are presented in a study by Khan et al., 2024 [43]. Particle size analysis using a Horiba LA-960 particle size distribution analyzer (Horiba, Ltd., Kyoto, Japan) revealed a gaussian distribution with D10, D50, and D90 values of 65 μm, 100 μm, and 190 μm. A histogram of particle size distribution for the algae powder used in this study can also be found in the study mentioned previously by Khan et al., 2024 [43]. Flowability was evaluated by measuring apparent density and repose angle using a Hall flowmeter (DF-1-02, HongTuo, Dongguan, GD, China) equipped with a Carney funnel, yielding values of 0.45 g/cm^3 and 56°, respectively. Referring to the flowability classification in Table 1, this indicated a "very cohesive" powder. Despite the relatively high cohesiveness, prior experiments confirmed that the powder was suitable for use with the ExOne Innovent+ printer [43].

2.4. Experimental Conditions

Three experimental conditions were used in this study:

- Condition 1, "No Auto-Stir": The ExOne Innovent+ OEM hopper was employed. This hopper did not involve stirring of the powder.

- Condition 2, "Auto-Stir Off": The custom-built hopper was employed. The screw augers remained inactive.
- Condition 3, "Auto-Stir On": The custom-built hopper was employed. The screw augers were active.

For all experiments conducted in this study, ultrasonic intensity of the ultrasonic vibration generator was set at 100%. The ramping pattern was set to "linear" and ramping speed was set to "normal"; detailed information on these parameters can be found in the literature [12,48]. Ultrasonic intensity, ramping pattern, and ramping speed were set based on preliminary trials which indicated these settings produced the most consistent powder dispensing, consistent with prior work using the same system [12,43,49]. All vibration parameters were then held constant throughout experimentation so that the effect of mechanical agitation could be isolated as the sole independent variable. ExOne Innovent+ printers have several screen options with varying mesh opening sizes to accommodate powders of different particle sizes. The V4 screen (circular mesh openings of 0.3 mm) was selected for this study based on preliminary trials, in which it produced consistent flowing of the powder from the hopper when the ultrasonic generator was active and reliably ceased flowing of the powder when it was deactivated. The temperature of the printer chamber was 23 °C ± 2 °C and the relative humidity was 35 ± 5%.

Three independent trials (duplications) were performed for each condition in a randomized order. In each trial, there was a series of cycles, each spanning 60 s. Each cycle was divided into 12 intervals, each interval spanning 5 s. Figure 5 provides a graphical overview of experimental design for this study.

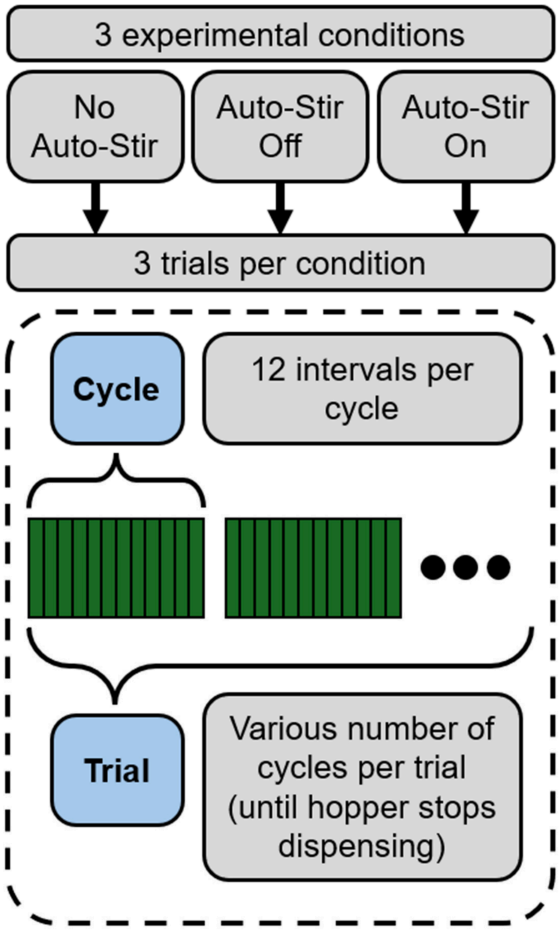

Figure 5. Graphical overview of experimental design for this study.

2.5. Measurement Setup for Dispensing Rate

The printing process for the ExOne Innovent+ involves hopper movement across the build platform during powder deposition. However, in this study, the hopper position was fixed to measure powder dispensing rate. The ExOne Innovent+ system has a "drain recoat" function that activates the ultrasonic generator while maintaining the hopper in a fixed position away from the build platform. Using this function, powder can be dispensed into a collection tray instead of being deposited on the build platform. Dispensing rate can be calculated from the measured mass of dispensed powder within a given period of time.

The use of a fixed hopper position is justified on the basis that gravity-driven hopper discharge rate is primarily governed by outlet geometry, powder properties, and gravitational pressure head rather than the lateral velocity of the hopper carriage [50]. This assumption is consistent with the approach taken by Wei et al., who characterized dispensing behavior of the ExOne Innovent+ hopper system under fixed conditions and drew conclusions applicable to the printing process [12]. The work by Wei et al. [12] establishes methodological precedent for static characterization on this machine; however, it does not constitute proof of physical equivalence between static and dynamic traverse conditions. For cohesive powders, lateral acceleration during traverse could in principle induce inertial compaction or asymmetric shear effects at the hopper outlet that are absent in a fixed-position setup. These effects are acknowledged as a limitation of the present study and are discussed further in Section 4.2.

Figure 6 shows the dispensing rate measurement setup. An Ohaus CS-5000 portable digital scale (capacity 5000 g, readability 1 g; Ohaus Corporation, Parsippany, NJ, USA) was placed directly beneath the hopper screen. The scale's 1 g resolution introduces quantization uncertainty into individual interval measurements, which is discussed as a limitation of the experimental setup in this study in Section 4.2. A stainless steel collection tray was set on the scale to measure the mass of dispensed powder. A smartphone (Apple iPhone 13, 12 MP rear camera, 60 fps; Apple Inc., Cupertino, CA, USA) was used to capture the video of the scale's digital display readout. The video provided a time-stamped record of cumulative mass throughout each dispensing cycle.

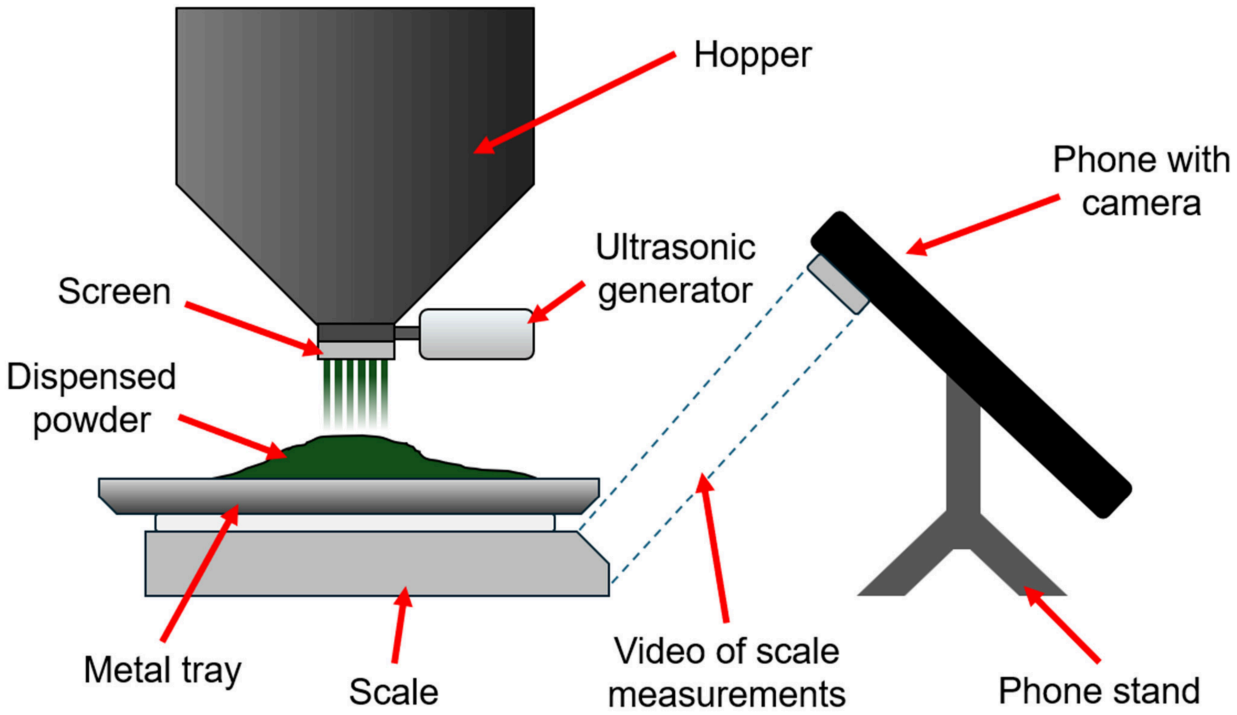

Figure 6. Illustration of the setup for measuring dispensing rate.

For each trial, the hopper was loaded with 1000 g of algae powder, the phone was mounted, the video recording was started, and the printer chamber door was closed. The drain recoat function was then executed for 60 s. When the dispensing cycle ended, the printer chamber door was opened to stop and restart the video recording on the phone. Then, the door was closed, and the drain recoat function was executed. These 60 s cycles were repeated until powder dispensing visibly ceased. If powder dispensing ceased before the completion of a drain recoat dispensing cycle, then the collected dispensing rate data for the cycle was not considered in analysis. The resulting series of 60 s videos constituted the data set used for dispensing rate analysis.

2.6. Measurement of Dispensing Rate Consistency

Each cycle (60 s long) was divided into 12 five-second intervals ($\Delta t = 5\,\mathrm{s}$). For each interval identified by i, the mass dispensed (Δm_i) was computed by subtracting the cumulative mass recorded at the start of the interval from the cumulative mass recorded at the end of the interval. The dispensing rate for each interval was calculated using Equation (1):

$$\dot{m}_i = \frac{\Delta m_i}{\Delta t} \tag{1}$$

To quantify dispensing rate consistency within a cycle, the standard deviation of the interval dispensing rates within each cycle ($\sigma_{\dot{m}_i}$) was calculated using Equation (2):

$$\sigma_{\dot{m}_i} = \sqrt{\frac{1}{N-1}\sum_{i=1}^{N}\left(\dot{m}_i - \overline{\dot{m}}\right)^2} \tag{2}$$

where $\overline{\dot{m}}$ was calculated with Equation (3) as:

$$\overline{\dot{m}} = \frac{1}{N}\sum_{i=1}^{N}\dot{m}_i \tag{3}$$

with $N = 12$ number of intervals in a cycle.

Smaller deviation within a cycle (i.e., lower value of $\sigma_{\dot{m}_i}$) indicates that powder dispensing rate was more consistent within a cycle. It measures the dispensing rate consistency between 12 intervals (each being five seconds long) within a cycle, revealing the short-term variability of dispensing rate.

To evaluate the long-term variability of dispensing rate, or the within-trial dispensing rate consistency, the pointwise deviation of dispensing rate for each interval was calculated using Equation (4):

$$\textit{Pointwise deviation} = \left|\dot{m}_i - \overline{\dot{m}}_{trial}\right| \tag{4}$$

where $\overline{\dot{m}}_{trial}$ is the mean of all the interval dispensing rates within a trial.

3. Results

3.1. Within-Cycle Dispensing Rate Consistency

Figure 7 compares within-cycle dispensing rate consistency among the three experimental conditions using boxplots. In the boxplot, each dot represents a single cycle's within-cycle standard deviation value, quantifying the short-term dispensing rate variability for that specific 60 s dispensing cycle. The location (central tendency) of the data is indicated by the thick horizontal median line in the middle of the box. The spread (dispersion) of the data is shown by multiple parameters: the box itself spans from the first quartile (Q1, the 25th percentile) to the third quartile (Q3, the 75th percentile), representing

the interquartile range (IQR) where the middle 50% of the data resides. The vertical whisker lines extend from the box to the minimum and maximum values within 1.5 × IQR from the quartiles, while dots appearing beyond the whiskers represent outliers.

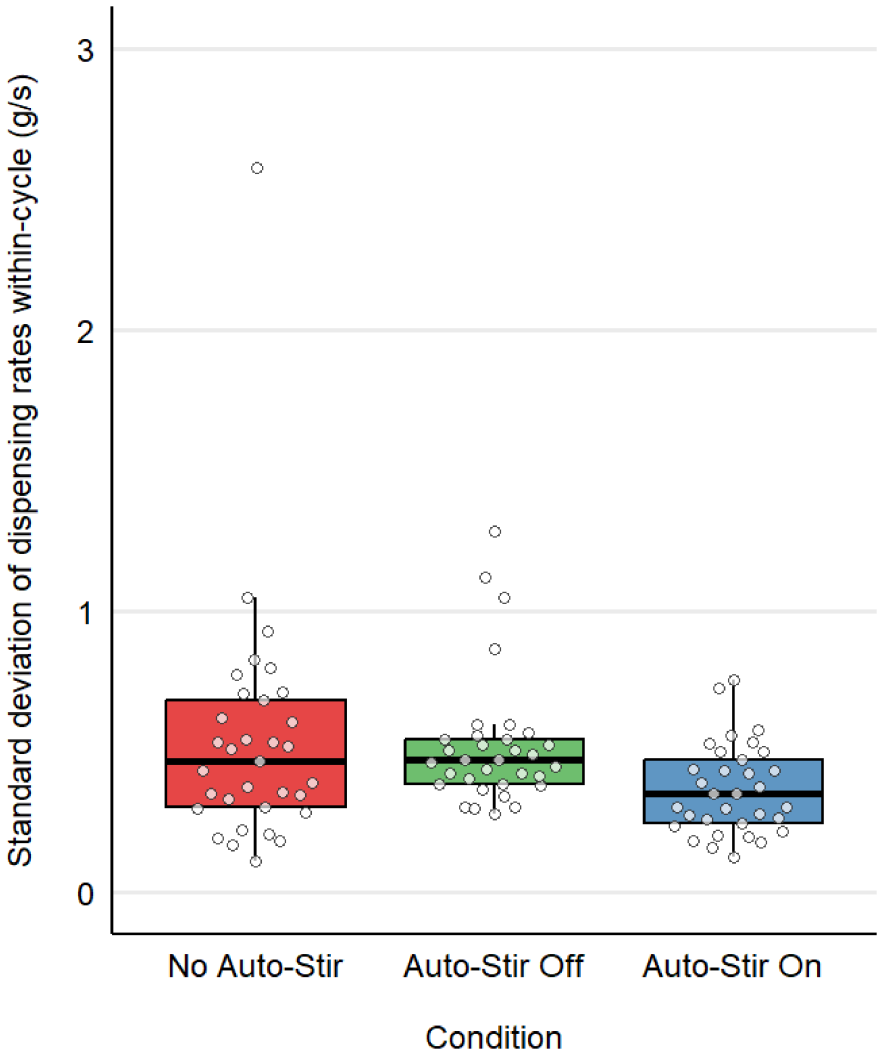

Figure 7. Comparison of within-cycle dispensing rate consistency among three experimental conditions.

The boxplot visually relays differences in both the location and spread of within-cycle standard deviation values among the three conditions. The median value for the "Auto-Stir On" condition (0.350 g/s) is smaller than those of the "No Auto-Stir" condition (0.463 g/s) and "Auto-Stir Off" condition (0.469 g/s). The "No Auto-Stir" condition has the widest spread and longest whiskers on either end, demonstrating the largest variance for within-cycle dispensing rate. The spread of the "Auto-Stir Off" condition is the tightest, yet the third quartile of the "Auto-Stir On" condition is below the median of the "Auto-Stir Off" condition. Although the IQR for the "Auto-Stir Off" condition is tighter than the "Auto-Stir On" condition, the location of the data for the "Auto-Stir On" condition is closer to zero. Additionally, the "Auto-Stir Off" condition displays multiple outliers beyond the upper whisker, visually emphasizing the presence of occasional cycles with particularly large fluctuations in dispensing rate. The "Auto-Stir On" condition does not exhibit outlier points.

Mean and standard deviation values of all the data for within-cycle deviation from three trials under each condition were calculated and included in Table 4. These statistics reveal the same trends as shown by the boxplots.

Table 4. Mean and standard deviation values of within-cycle dispensing rate consistency.

Condition	Mean (g/s)	Standard Deviation (g/s)
No Auto-Stir	0.542	0.435
Auto-Stir Off	0.521	0.233
Auto-Stir On	0.364	0.159

The data from the "Auto-Stir On" condition had the lowest mean standard deviation value (0.364 g/s), while the data from the "No Auto-Stir" and "Auto-Stir Off" conditions had similar mean standard deviation values (0.542 g/s and 0.521 g/s, respectively). In terms of short-term dispensing rate consistency, the "Auto-Stir On" condition increased the within-cycle dispensing rate consistency by 33% compared with the "No Auto-Stir" condition and 30% compared with the "Auto-Stir Off" condition. Additionally, the data from the "Auto-Stir On" condition showed the lowest variability (standard deviation of within-cycle deviation values), with a standard deviation value of 0.159 g/s. The variability of the data from the "No Auto-Stir" and "Auto-Stir Off" conditions was higher, with standard deviation values of 0.435 g/s and 0.233 g/s, respectively.

Tukey's honestly significant difference post hoc test was performed on all pairwise comparisons (Table 5). The results reveal that the "Auto-Stir On" condition produced significantly lower within-cycle variability compared with the "No Auto-Stir" condition ($p = 0.046$), indicating that active mechanical agitation enhances short-term dispensing rate consistency at the significance level of $\alpha = 0.05$. The difference between the "Auto-Stir Off" condition and the "Auto-Stir On" condition was not statistically significant at the significance level of $\alpha = 0.05$ (because $p = 0.088$) but would be statistically significant at a marginal significance level (such as $\alpha = 0.10$). The "No Auto-Stir" condition and the "Auto-Stir Off" condition showed no significant difference ($p = 0.958$), indicating that the mere presence of inactive augers within the hopper does not alter dispensing behavior.

Table 5. *p*-Values from Tukey's honestly significant difference test for within-cycle dispensing rate consistency.

Configuration Comparison	*p*-Value
No Auto-Stir vs. Auto-Stir Off	0.958
Auto-Stir Off vs. Auto-Stir On	0.088
No Auto-Stir vs. Auto-Stir On	0.046

3.2. Within-Trial Dispensing Rate Consistency

Figure 8 presents a boxplot of within-trial dispensing rate consistency by experimental condition. In this visualization, each dot represents a single five-second interval's pointwise deviation value calculated using Equation (4), quantifying how far that specific interval's dispensing rate deviates from the overall trial mean dispensing rate. The boxplot elements (median, quartiles, IQR, whiskers, and outliers) are interpreted using the same conventions described in Section 3.1. Mean and standard deviation values for within-trial deviation data were also calculated; the values are provided in Table 6.

The boxplot shows differences in both the location and spread of pointwise deviation values among the three conditions. The median value for the "Auto-Stir On" condition (0.155 g/s) is closer to zero than those of the "No Auto-Stir" (0.282 g/s) and "Auto-Stir Off" (0.338 g/s) conditions. The "Auto-Stir On" condition exhibits the most compact distribution, with the shortest IQR indicating that interval dispensing rates consistently remain close to the trial median. In contrast, the "No Auto-Stir" and "Auto-Stir Off" conditions display taller boxes and more widely distributed data points, reflecting greater long-term variability

in dispensing rate consistency. This pattern demonstrates that active mechanical agitation not only reduces the magnitude of deviations but also constrains the range of variability across extended dispensing operations.

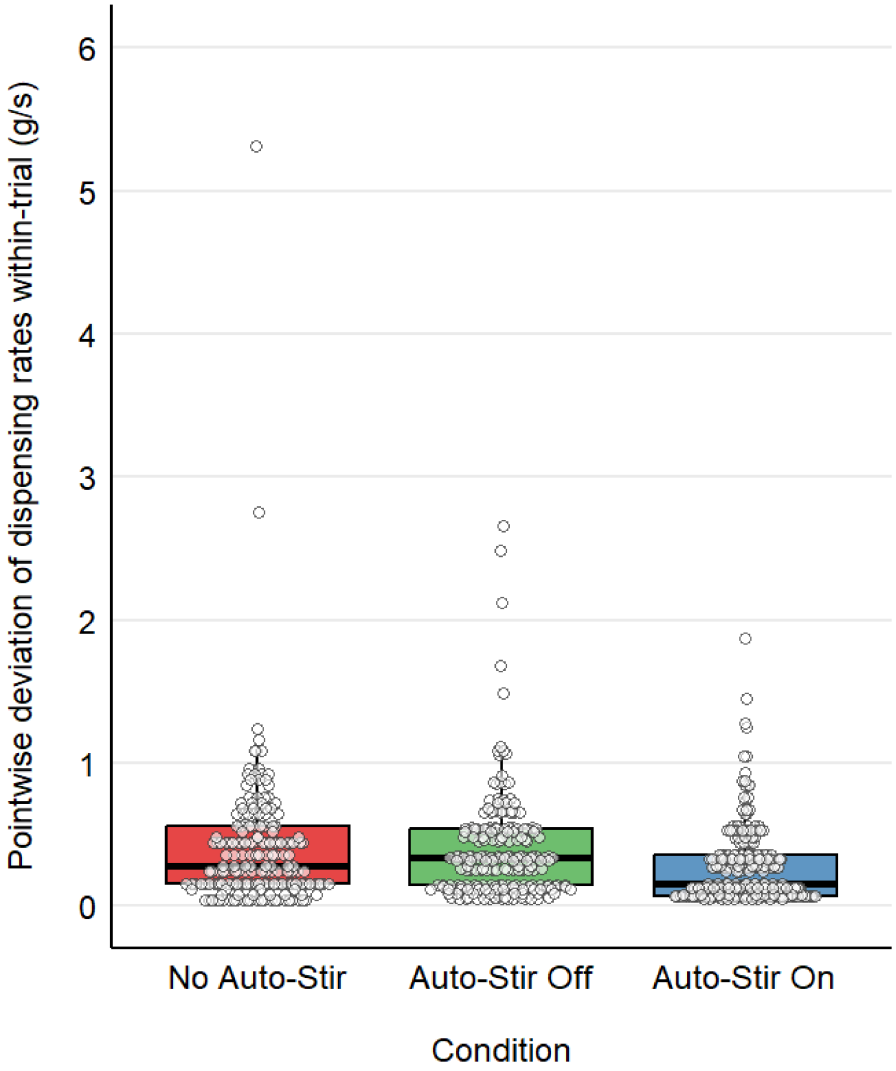

Figure 8. Boxplot of within-trial dispensing rate consistency by experimental condition.

Table 6. Mean and standard deviation of within-trial dispensing rate.

Condition	Mean (g/s)	Standard Deviation (g/s)
No Auto-Stir	0.405	0.500
Auto-Stir Off	0.399	0.380
Auto-Stir On	0.274	0.255

The "Auto-Stir On" condition had the lowest mean pointwise deviation value at 0.274 g/s, while "No Auto-Stir" and "Auto-Stir Off" had mean pointwise deviation values of 0.405 g/s and 0.399 g/s, respectively. In terms of long-term dispensing rate consistency enhancement, "Auto-Stir On" increased the within-trial dispensing rate consistency by 32% compared to "No Auto-Stir" and 31% compared to "Auto-Stir Off". The "Auto-Stir On" condition had the lowest variability, with a standard deviation of pointwise deviation of 0.255 g/s. The variability of "No Auto-Stir" and "Auto-Stir Off" was higher, with values of 0.500 g/s and 0.380 g/s.

Tukey's honestly significant difference (HSD) post hoc test was performed on all pairwise comparisons (Table 7). The results reveal that the "Auto-Stir On" condition produced significantly lower within-trial variability compared with both the "No Auto-Stir" condition (p = 0.001) and the "Auto-Stir Off" condition (p = 0.002), indicating that active mechanical agitation substantially enhances long-term dispensing rate consistency at the significance level of α = 0.05. The "No Auto-Stir" condition and the "Auto-Stir Off" condition showed no significant difference (p = 0.984), consistent with the within-cycle findings and further confirming that the mere presence of inactive augers within the hopper does not alter dispensing behavior. The stronger statistical significance observed in the within-trial framework compared to within-cycle comparisons suggests that mechanical agitation's impact on dispensing consistency is more substantial for long-term operation than for short-term fluctuations.

Table 7. *p*-Values from Tukey's honestly significant difference for within-trial dispensing rate consistency.

Configuration Comparison	*p*-Value
No Auto-Stir vs. Auto-Stir Off	0.984
Auto-Stir Off vs. Auto-Stir On	0.002
No Auto-Stir vs. Auto-Stir On	0.001

4. Discussion

4.1. Mechanistic Interpretation of Dispensing Rate Consistency Improvement

Several common issues contributing to inconsistent powder dispensing in hopper-based dispensing systems have been identified in the literature [34]. Arching or bridging phenomena, where stable powder structures form across hopper outlets, can completely halt powder flow and require external intervention [33,51]. Ratholing, where powder flows preferentially through central channels, can lead to stagnant zones and inconsistent discharge rates [52,53]. Irregular flow is characterized by inconsistent discharge rates due to factors such as fluctuations in powder cohesion, particle properties, moisture, or non-ideal hopper geometry, resulting in unpredictable and inconsistent flow events [35]. Segregation, the tendency of powder components with different size, shape, or density to separate during hopper filling or discharge, often arises in funnel flow hoppers and can produce significant disparities in composition and product uniformity at the outlet [54]. These issues are exacerbated by the relatively small outlet dimensions typically employed in hopper-based binder jetting 3D printers [38,55]. The results of this study suggest that active mechanical agitation can mitigate phenomena that contribute to inconsistent dispensing rates, such as arching, ratholing, and irregular flow. However, the continuous application of shear forces may amplify segregation tendencies, and further investigation is needed to confirm these relationships.

The observed improvement in dispensing rate consistency with the "Auto-Stir ON" condition can be attributed to several mechanistic factors related to the processing of cohesive powders. The counter-rotating screw augers generate opposing flow fields that converge toward the hopper center, creating continuous shear-induced mixing within the powder bed. This agitation disrupts the formation of stable powder structures that commonly develop in cohesive materials [33,51–53].

Within-cycle boxplots (Figure 7) show that the "Auto-Stir Off" condition has a slightly tighter IQR than "Auto-Stir On," but a higher median deviation and more high-magnitude outliers. This pattern may support the notion that inactive augers modify the internal flow paths of the feedstock powder inside the hopper, constraining lateral powder movement without reducing the typical deviation from the mean dispensing rate. As a result, fluctuations appear somewhat compressed while intermittent large deviations still occur.

The algae powder employed in this study exhibited "very cohesive" flow characteristics. Under static conditions, such powders tend to form preferential flow channels and stagnant zones that contribute to inconsistent dispensing rates. The mechanical agitation provided by the auto-stir system continuously disrupts these structures, promoting more uniform powder movement toward the hopper outlet. The absence of significant improvement in the "Auto-Stir Off" scenario, despite otherwise identical geometry, further isolates the mechanism: it is the mechanical action of agitation, not merely the presence of additional hardware or alternate mass distribution, that delivers enhanced dispensing rate consistency.

4.2. Limitations of the Study

This section discusses key limitations of the experimental design and measurement methodology that contextualize the findings reported above. It should be noted that the ultrasonic generator was active for all three experimental conditions. Ultrasonic vibration is a functional requirement of the ExOne Innovent+ hopper dispensing mechanism, without which powder does not flow through the screen. Thus, it is not a controllable independent variable in this system. A vibration-off condition is therefore physically impractical and was not included. Consequently, the effects observed in this study reflect the contribution of mechanical agitation beyond what ultrasonic vibration alone provides, rather than the isolated effect of mechanical agitation in the absence of vibration. A related limitation concerns the use of a fixed hopper position during dispensing rate measurement. While static testing is reasonable based on the gravity-driven discharge theory and is consistent with prior work on this printer, the static setup does not capture potential traverse-induced effects such as inertial compaction or asymmetric shear at the hopper outlet that may arise during actual printing. Whether these dynamic effects alter the relative performance of the auto-stir system compared to the standard hopper remains an open question that future work should address through dynamic traverse testing.

Another limitation of this study concerns the resolution of the measurement instrument. The Ohaus CS-5000 scale, with a resolution of 1 g, was used to measure dispensed mass over 5 s intervals. Given the measured dispensing rates of approximately 0.3–0.5 g/s, each interval yielded approximately 1.5–2.5 g of powder. At 1 g resolution, a relative quantization uncertainty of approximately 40–65% per interval was introduced. This quantization uncertainty could have inflated the apparent within-cycle and within-trial standard deviation values across all conditions. However, because the same instrument and interval duration were applied across all three experimental conditions, any systematic bias introduced by the measurement resolution affected all conditions. It should also be noted that the Tukey HSD test was not applied to individual interval dispensing rates directly, but to within-cycle standard deviations derived from 12 aggregated interval measurements per cycle, and to within-trial pointwise deviations aggregated across all intervals in a trial. Aggregating over multiple intervals substantially reduces the influence of single-interval quantization error on the summary statistics used in the statistical tests. Because quantization noise is random and symmetric, any resulting inflation of variance affects all three conditions approximately equally, making the statistical tests conservative. The within-trial Tukey HSD results (No Auto-Stir vs. Auto-Stir On: $p = 0.001$; Auto-Stir Off vs. Auto-Stir On: $p = 0.002$), based on a substantially larger number of observations, corroborate the results from within-cycle data ($p = 0.046$). The convergence of both within-cycle and within-trial data on the same directional finding provides a certain level of confidence in the drawn conclusions. Future work should employ a higher resolution scale (e.g., 0.1 g or 0.01 g resolution) or longer measurement intervals to reduce relative quantization uncertainty.

A further limitation concerns the environmental conditioning of the feedstock powder prior to testing. While the printer chamber temperature (23 °C ± 2 °C) and relative humidity (35 ± 5%) were monitored and reported, and the algae powder was stored consistently in a controlled laboratory environment between trials, no formal powder equilibration protocol was employed. Additionally, moisture content was not independently measured via Karl Fischer titration [56] or loss-on-drying [57]. For highly cohesive powders such as the algae powder used in this study, residual moisture and triboelectric charge state are known to influence interparticle cohesive forces and, consequently, flow behavior. The absence of a controlled equilibration period means that inter-trial variability in powder moisture state may have contributed to the observed variability in dispensing rate across trials. Similarly, no explicit static charge dissipation protocol was applied between trials, which may have introduced additional variability given the susceptibility of cohesive powders to triboelectric charging. To block these effects, a randomized order of experimental trials was employed. Doing so could distribute any time-dependent drift in powder moisture or triboelectric state across all three conditions, reducing the likelihood of systematic bias. The absence of a statistically significant difference between the No Auto-Stir and Auto-Stir Off conditions (p = 0.958 within-cycle; p = 0.984 within-trial) provides indirect evidence that inter-trial variability in powder state did not systematically confound the observed effect of active mechanical agitation. However, future work should incorporate a standardized powder equilibration period, moisture content verification, and anti-static measures prior to each trial to improve reproducibility and enable more direct comparison across experimental conditions.

4.3. Practical Engineering Implications and Future Work

The auto-stir system in this study was evaluated using only algae powder. Future work should systematically test a variety of feedstock powders, spanning a range of flowability classifications. Based on the flowability data presented in Table 3, metal powders commonly used in binder jetting 3D printing, which exhibit free-flowing characteristics with repose angles below 40°, do not require the mechanical agitation applied to the highly cohesive algae powder used in this study. However, ceramic powders with cohesive or fair-flow classifications, such as spherical alumina (repose angle ~50°), would be expected to show meaningful improvement in dispensing rate consistency with active auto-stirring agitation, though this remains to be experimentally verified.

Practically, the modular design of the auto-stir hopper, which preserves the OEM hopper envelope, suggests that active mechanical agitation can be retrofitted to existing hopper-based binder jetting systems with minimal modification. The absence of a significant difference between the "No Auto-Stir" and "Auto-Stir Off" conditions indicates that performance gains arise from active agitation rather than geometric changes, identifying agitation as a design improvement for future hopper systems. Subsequent studies should link dispensing rate consistency more directly to printed part outcomes, including layer density uniformity, dimensional accuracy, and mechanical properties. Additional attention could also be directed toward the characterization of powder flow dynamics on the particle level, as this study did not investigate shear flow mechanics.

5. Conclusions

This study evaluated the effects of a custom-built auto-stir hopper on powder dispensing rate consistency in hopper-based binder jetting 3D printing using very cohesive algae powder. Based on the results, the following conclusions were drawn:

- The auto-stir hopper with active mechanical agitation ("Auto-Stir On"), in addition to ultrasonic vibration, reduced within-cycle standard deviation of dispensing rate

by about one-third relative to the OEM hopper ("No Auto-Stir"), indicating more consistent dispensing rates short-term.

- Analysis of within-trial pointwise deviations showed a reduction in long-term dispensing rate variability under the "Auto-Stir On" condition, indicating more consistent dispensing rates long-term.
- A Tukey post hoc test revealed that the "Auto-Stir On" condition significantly improved dispensing rate consistency compared with the "No Auto-Stir" condition at the 0.05 significance level both short-term (p = 0.046) and long-term (p = 0.001). The "Auto-Stir Off" condition showed no significant difference from "No Auto-Stir" ($p > 0.95$) in both within-cycle and within-trial cases, isolating mechanical agitation as the key factor driving the enhancement of dispensing rate consistency.
- These findings were derived from experiments using a cohesive organic powder (algae with a repose angle of 56°) and may not be directly applicable to free-flowing metal or ceramic feedstocks without additional experimental validation.

The results indicate that the combination of ultrasonic vibration and mechanical agitation can be effective in enhancing powder dispensing rate consistency in hopper-based binder jetting printers. Future work should evaluate this approach with additional powder types and directly link improved dispensing rate consistency to printed part quality such as density, dimensional accuracy, and mechanical properties.

Author Contributions: Conceptualization: J.S., S.K., Z.P., Y.-T.K. and K.D. contributed to developing the research concept and defining the study objectives. Methodology: J.S. and S.K. designed the experimental methodology and the auto-stir hopper system. Software: S.K. developed and implemented the software and control code. Investigation: J.S. and S.K. conducted the experiments and collected the data. Data curation: J.S. and S.K. organized and curated the experimental data. Formal analysis: J.S. performed the statistical analysis and interpretation of the results. Resources: Z.P. provided key resources, including equipment and facilities. Supervision: Z.P., Y.-T.K. and K.D. provided technical guidance. Visualization: J.S. prepared the figures and tables. Writing—original draft: J.S. wrote the main manuscript text. Writing—review and editing: Z.P. and Y.-T.K. provided primary edits and revisions to the manuscript. All authors reviewed the manuscript. All authors have read and agreed to the published version of the manuscript.

Funding: No external financial support or grants were received for the conduct of this research or the preparation of this manuscript.

Data Availability Statement: The original contributions presented in this study are included in the article. Further inquiries can be directed to the corresponding author.

Conflicts of Interest: Authors Yi-Tang Kao and Kenneth Dubovick were employed by Saint-Gobain Research North America. Author Siddhartha Kazi was a student at Texas A&M University during the experimentation and initial draft writing phase; at the time of manuscript submission, he was employed by Molex. The remaining authors declare that they have no competing financial or non-financial interests as defined by MDPI, or other interests that might be perceived to influence the results and/or discussion reported in this paper.

References

1. Dev Singh, D.; Mahender, T.; Raji Reddy, A. Powder Bed Fusion Process: A Brief Review. *Mater. Today Proc.* **2021**, *46*, 350–355. [CrossRef]
2. Ziaee, M.; Crane, N.B. Binder Jetting: A Review of Process, Materials, and Methods. *Addit. Manuf.* **2019**, *28*, 781–801. [CrossRef]
3. Abd-Elaziem, W.; Elkatatny, S.; Abd-Elaziem, A.-E.; Khedr, M.; Abd El-baky, M.A.; Hassan, M.A.; Abu-Okail, M.; Mohammed, M.; Järvenpää, A.; Allam, T.; et al. On the Current Research Progress of Metallic Materials Fabricated by Laser Powder Bed Fusion Process: A Review. *J. Mater. Res. Technol.* **2022**, *20*, 681–707. [CrossRef]

4. Davoodi, F.; Varmaziar, S.; Atapour, M.; Iuliano, L.; Saboori, A. In Vitro Corrosion and Bio-Tribocorrosion Performance of Electron Beam Powder Bed Fusion Ti6Al4V Specimens with Lapping and Superfinishing Treatments. *Prog. Addit. Manuf.* **2025**, *10*, 9117–9132. [CrossRef]
5. Dejene, N.D.; Lemu, H.G. Current Status and Challenges of Powder Bed Fusion-Based Metal Additive Manufacturing: Literature Review. *Metals* **2023**, *13*, 424. [CrossRef]
6. Gaikwad, M.U.; Gaikwad, P.U.; Ambhore, N.; Sharma, A.; Bhosale, S.S. Powder Bed Additive Manufacturing Using Machine Learning Algorithms for Multidisciplinary Applications: A Review and Outlook. *Recent Pat. Mech. Eng.* **2025**, *18*, 12–25. [CrossRef]
7. Katz-Demyanetz, A.; Popov, V.V.; Kovalevsky, A.; Safranchik, D.; Koptyug, A. Powder-Bed Additive Manufacturing for Aerospace Application: Techniques, Metallic and Metal/Ceramic Composite Materials and Trends. *Manuf. Rev.* **2019**, *6*, 5. [CrossRef]
8. Salehi, H.; Cummins, J.; Gallino, E.; Garg, V.; Deng, T.; Hassanpour, A.; Bradley, M. Optimising Spread-Layer Quality in Powder Additive Manufacturing: Assessing Packing Fraction and Segregation Tendency. *Processes* **2023**, *11*, 2276. [CrossRef]
9. Moghadasi, M.; Du, W.; Li, M.; Pei, Z.; Ma, C. Ceramic Binder Jetting Additive Manufacturing: Effects of Particle Size on Feedstock Powder and Final Part Properties. *Ceram. Int.* **2020**, *46*, 16966–16972. [CrossRef]
10. Wang, L.; Wu, H.; Yin, Z.; Jiang, C.; Pan, Y.; He, L.; Nie, G.; Deng, X.; Wu, S. Additive Manufacturing of High-Performance SiO_2-Al_2O_3-K_2O (Na_2O) Ceramic Components via Binder Jetting Technology. *Ceram. Int.* **2025**, *51*, 529–540. [CrossRef]
11. Miao, G.; Du, W.; Pei, Z.; Ma, C. A Literature Review on Powder Spreading in Additive Manufacturing. *Addit. Manuf.* **2022**, *58*, 103029. [CrossRef]
12. Wei, X.; Moghadasi, M.; Du, W.; Ma, C.; Pei, Z. Experimental Investigation on Ultrasonic Hopper Dispensing System in Powder Bed Additive Manufacturing. *J. Manuf. Process.* **2021**, *71*, 106–112. [CrossRef]
13. Li, Z.; Li, H.; Yin, J.; Li, Y.; Nie, Z.; Li, X.; You, D.; Guan, K.; Duan, W.; Cao, L.; et al. A Review of Spatter in Laser Powder Bed Fusion Additive Manufacturing: In Situ Detection, Generation, Effects, and Countermeasures. *Micromachines* **2022**, *13*, 1366. [CrossRef]
14. Meier, C.; Fuchs, S.L.; Much, N.; Nitzler, J.; Penny, R.W.; Praegla, P.M.; Proell, S.D.; Sun, Y.; Weissbach, R.; Schreter, M.; et al. Physics-Based Modeling and Predictive Simulation of Powder Bed Fusion Additive Manufacturing Across Length Scales. *GAMM-Mitteilungen* **2021**, *44*, e202100014. [CrossRef]
15. Lampitella, V.; Trofa, M.; Astarita, A.; D'Avino, G. Discrete Element Method Analysis of the Spreading Mechanism and Its Influence on Powder Bed Characteristics in Additive Manufacturing. *Micromachines* **2021**, *12*, 392. [CrossRef] [PubMed]
16. Chen, Y.; Wang, Y.; Huang, L.; Su, B.; Yang, Y. Investigating the Microscopic Mechanism of Ultrasonic-Vibration-Assisted-Pressing of WC-Co Powder by Simulation. *Materials* **2023**, *16*, 5199. [CrossRef]
17. Sinclair, C.W.; Edinger, R.; Sparling, W.; Molavi-Kakhki, A.; Labrecque, C. Vibratory Powder Feeding for Powder Bed Additive Manufacturing Using Water and Gas Atomized Metal Powders. *Materials* **2021**, *14*, 3548. [CrossRef]
18. Kollmann, T.H.; Tomas, J. Effect of Applied Vibration on Silo Hopper Design. *Part. Sci. Technol.* **2002**, *20*, 15–31. [CrossRef]
19. Shah, D.S.; Moravkar, K.K.; Jha, D.K.; Lonkar, V.; Amin, P.D.; Chalikwar, S.S. A Concise Summary of Powder Processing Methodologies for Flow Enhancement. *Heliyon* **2023**, *9*, e16498. [CrossRef]
20. Jallo, L.J.; Ghoroi, C.; Gurumurthy, L.; Patel, U.; Davé, R.N. Improvement of Flow and Bulk Density of Pharmaceutical Powders Using Surface Modification. *Int. J. Pharm.* **2012**, *423*, 213–225. [CrossRef]
21. Kunnath, K.T.; Tripathi, S.; Kim, S.S.; Chen, L.; Zheng, K.; Davé, R.N. Selection of Silica Type and Amount for Flowability Enhancements via Dry Coating: Contact Mechanics Based Predictive Approach. *Pharm. Res.* **2023**, *40*, 2917–2933. [CrossRef]
22. Chattoraj, S.; Shi, L.; Sun, C.C. Profoundly Improving Flow Properties of a Cohesive Cellulose Powder by Surface Coating with Nano-silica through Comilling. *J. Pharm. Sci.* **2011**, *100*, 4943–4952. [CrossRef]
23. Lu, G.; Zhao, J.; Zhou, Y.; Fu, Y.; Lu, S.; Zhang, H. Study on Flowability Enhancement and Performance Testing of Ultrafine Dry Powder Fire Extinguishing Agents Based on Application Requirements. *Fire* **2024**, *7*, 146. [CrossRef]
24. Janzen, K.; Kallies, K.J.; Waalkes, L.; Imgrund, P.; Emmelmann, C. Influence of Different Powder Conditioning Strategies on Metal Binder Jetting with Ti-6Al-4V. *Materials* **2024**, *17*, 750. [CrossRef]
25. Rescaglio, A.; De Smet, F.; Aerts, L.; Lumay, G. Tribo-Electrification of Pharmaceutical Powder Blends. *Part. Sci. Technol.* **2019**, *37*, 1024–1031. [CrossRef]
26. Gao, G.; Zhang, X.; Xu, M.; Han, Y.; Ao, J.; Cai, Y.; Wang, J. Structural Optimized Design of a Powder Mixer for Multi-Material Directed Energy Deposition Based on CFD-DPM. *Coatings* **2023**, *13*, 773. [CrossRef]
27. Badgujar, C.M.; Wu, H.; Flippo, D.; Brokesh, E. Design, Fabrication, and Experimental Investigation of Screw Auger Type Feed Mechanism for a Robotic Wheat Drill. *J. ASABE* **2022**, *65*, 1333–1342. [CrossRef]
28. Bai, P.; Yang, S.; Yan, Y.; Wang, D.; Ma, Y. Advances in Powder-Filled Mold Processes: A Comprehensive Review and Outlook. *Materials* **2024**, *17*, 5476. [CrossRef] [PubMed]
29. Nicolai, R.; Ollerich, J.; Kelley, J. Screw Auger Power and Throughput Analysis. In Proceedings of the 2004 ASAE Annual Meeting, Ottawa, ON, Canada, 1–4 August 2004.

30. Ghosh, B.N. Conveyance of Wet Parchment Coffee Beans by an Auger. *J. Agric. Eng. Res.* **1967**, *12*, 274–280. [CrossRef]
31. Williams, D.F.; Lofgren, C.S.; Plumley, J.K.; Hicks, D.M. Auger-Applicator for Applying Small Amounts of Granular Pesticides. *J. Econ. Entomol.* **1983**, *76*, 395–397. [CrossRef]
32. Dunst, P.; Bornmann, P.; Hemsel, T.; Sextro, W. Vibration-Assisted Handling of Dry Fine Powders. *Actuators* **2018**, *7*, 18. [CrossRef]
33. Lopes Neto, J.P.; do Nascimento, J.W.B.; Silva, R.C.; da Costa, C.A. Powder Flow Criteria for Design of Vertical Silo Walls. *Eng. Agríc.* **2013**, *33*, 453–462. [CrossRef]
34. Schulze, D. *Powders and Bulk Solids: Behavior, Characterization, Storage and Flow*; Springer International Publishing: Cham, Switzerland, 2021.
35. Mehos, G.; Morgan, D. Hopper Design Principles. *Chem. Eng.* **2016**, *123*, 58.
36. Cleary, P.W.; Sawley, M.L. DEM Modelling of Industrial Granular Flows: 3D Case Studies and the Effect of Particle Shape on Hopper Discharge. *Appl. Math. Model.* **2002**, *26*, 89–111. [CrossRef]
37. McGlinchey, D. (Ed.) *Bulk Solids Handling*, 1st ed.; John Wiley & Sons, Ltd.: Hoboken, NJ, USA, 2008.
38. Das, S.; Santosa, J. Design of a Micro-Hopper Array for Multi-Material Powder Deposition. In Proceedings of the International Solid Freeform Fabrication Symposium, Austin, TX, USA, 6–8 August 2001; pp. 155–162. [CrossRef]
39. Wang, H.; Zhang, T.; Zhao, M.; Chen, R.; Wu, L. Micro-Dosing of Fine Cohesive Powders Actuated by Pulse Inertia Force. *Micromachines* **2018**, *9*, 73. [CrossRef] [PubMed]
40. Jansen, D.; Hanemann, T.; Radek, M.; Rota, A.; Schröpfer, J.; Heilmaier, M. Development of Actual Powder Layer Height Depending on Nominal Layer Thicknesses and Selection of Laser Parameters. *J. Mater. Process. Technol.* **2021**, *298*, 117305. [CrossRef]
41. Oropeza, D.; Roberts, R.; Hart, A.J. A Modular Testbed for Mechanized Spreading of Powder Layers for Additive Manufacturing. *Rev. Sci. Instrum.* **2021**, *92*, 015114. [CrossRef]
42. Zhou, W.; Chen, P.; Min, M.; Ma, X.; Wang, J.; Griffith, R.; Hussain, F.; Peng, P.; Xie, Q.; Li, Y.; et al. Environment-Enhancing Algal Biofuel Production Using Wastewaters. *Renew. Sustain. Energy Rev.* **2014**, *36*, 256–269. [CrossRef]
43. Khan, F.; Shakil Arman, M.; Sanders, J.; Meraj Pasha, M.; Mazedur Rahman, A.; Pei, Z.; Dong, T. Binder Jetting 3D Printing Utilizing Waste Algae Powder: A Feasibility Study. *Intell. Sustain. Manuf.* **2024**, *1*, 10016. [CrossRef]
44. Zegzulka, J.; Gelnar, D.; Jezerska, L.; Prokes, R.; Rozbroj, J. Characterization and Flowability Methods for Metal Powders. *Sci. Rep.* **2020**, *10*, 21004. [CrossRef]
45. Reddy, R.S.; Ramachandra, C.T.; Hiregoudar, S.; Nidoni, U.; Ram, J.; Kammar, M. Influence of Processing Conditions on Functional and Reconstitution Properties of Milk Powder Made from Osmanabadi Goat Milk by Spray Drying. *Small Rumin. Res.* **2014**, *119*, 130–137. [CrossRef]
46. Oropeza, D.; Penny, R.W.; Gilbert, D.; Hart, A.J. Mechanized Spreading of Ceramic Powder Layers for Additive Manufacturing Characterized by Transmission X-Ray Imaging: Influence of Powder Feedstock and Spreading Parameters on Powder Layer Density. *Powder Technol.* **2022**, *398*, 117053. [CrossRef]
47. Oh, J.-W.; Park, J.; Nahm, S.; Choi, H. SiC-Si Composite Part Fabrication via SiC Powder Binder Jetting Additive Manufacturing and Molten-Si Infiltration. *Int. J. Refract. Met. Hard Mater.* **2021**, *101*, 105686. [CrossRef]
48. Sonia, P.; Jain, J.K.; Saxena, K.K. Influence of Ultrasonic Vibration Assistance in Manufacturing Processes: A Review. *Mater. Manuf. Process.* **2021**, *36*, 1451–1475. [CrossRef]
49. Li, M.; Miao, G.; Du, W.; Pei, Z.; Ma, C. Difference between Powder Bed Density and Green Density for a Free-Flowing Powder in Binder Jetting Additive Manufacturing. *J. Manuf. Process.* **2022**, *84*, 448–456. [CrossRef]
50. Hilton, J.E.; Cleary, P.W. Granular Flow during Hopper Discharge. *Phys. Rev. E* **2011**, *84*, 011307. [CrossRef]
51. Park, H.W.; Kim, S.T.; Choung, M.G.; Han, W.-Y.; Yoon, W.B. Analysis of Grinding Kinetics and Flow Behavior of Adzuki Bean (*Phaseolus angularis*) Flour for Hopper Design. *J. Food Process Eng.* **2016**, *39*, 366–376. [CrossRef]
52. Hidaka, J.; Kano, J.; Shimosaka, A. Flow Mechanism of Granular Materials Discharging from Bin-Hopper System. *KONA Powder Part. J.* **1995**, *13*, 205–213. [CrossRef]
53. Timoleanov, K.; Savenkov, D.; Gorgadze, L. Features of Designing Feeding Hoppers of Loose Materials of Low Productivity in Agriculture. *MATEC Web Conf.* **2018**, *224*, 05020. [CrossRef]
54. Jakubowska, E.; Ciepluch, N. Blend Segregation in Tablets Manufacturing and Its Effect on Drug Content Uniformity—A Review. *Pharmaceutics* **2021**, *13*, 1909. [CrossRef]
55. Mann, M.; Davies, R.; Lawrence, C.; Ghita, O. Prototype Design for Grading Structures in Powder Bed Fusion Processes. *3D Print. Addit. Manuf.* **2023**, *10*, 1320–1335. [CrossRef]

56. Mellin, P.; Zavalis, T.; Tingö, L.; Brodin, H.; Wendel, J.; Berg, S.; Riabov, D.; Strondl, A.; Nyborg, L. Moisture Content Analysis of Metal Powders Using Oven Desorption Followed by Karl Fischer Titration. *Met. Powder Rep.* **2020**, *75*, 34–39. [CrossRef]
57. Ileleji, K.E.; Garcia, A.A.; Kingsly, A.R.P.; Clementson, C.L. Comparison of Standard Moisture Loss-on-Drying Methods for the Determination of Moisture Content of Corn Distillers Dried Grains with Solubles. *J. AOAC Int.* **2010**, *93*, 191–196. [CrossRef]